Control and Modulation Methods of Single-/Three-Phase PWM Converter for Suppressing Leakage Current

Juwon Lee, *Student Member, IEEE*, Dongsu Lee, *Student Member, IEEE*, and Jung-Ik Ha, *Fellow, IEEE*

***Abstract*—Transformerless power converters are increasingly getting attention in the ac–dc power conversion due to their advantages in improving the efficiency and the power density. However, the removal of the isolation barrier with high common-mode (CM) impedance generates a leakage current issue due to the common-mode voltage (CMV), posing a human safety risk. This article comprehensively analyzes the influence of the CMV sources on the leakage currents, dividing into the low- and high-frequency (HF) components. To this end, a CM equivalent circuit is developed, considering the filter and grounding system. In order to mitigate the low-frequency (LF) leakage currents, a CMV control method is proposed, which generates the LF CMV through the pulsewidth modulation (PWM) converters. The leakage current flowing into the ground wire is directly measured and utilized as a feedback for the controller. Subsequently, a high-dimensional space vector PWM (HDSVPWM) is introduced to synthesize both differential mode voltage and CMV references for the single-/three-phase PWM converter. The proposed HDSVPWM minimizes the HF CMV ripple, reducing the HF leakage currents. The effectiveness of the proposed control and modulation methods is verified with an experimental setup of grid-connected transformerless PWM converter, ensuring a compliance with the safety regulations.**

***Index Terms*—AC–DC power conversion, common-mode voltage (CMV), leakage current, pulsewidth modulation (PWM), transformerless converter.**

I. Introduction

AC–DC power conversion is widely utilized across a spectrum of applications, from low-power to high-power systems, including charging infrastructure [1], grid interface converter [2], and renewable energy systems [3]. As electric vehicles (EV) and microgrids have emerged as key technologies in response to the global climate policies, the demand for the single-phase or three-phase grid-connected ac–dc converter has been increasing significantly.

Received 15 September 2024; revised 17 January 2025; accepted 21 February 2025. Date of publication 27 February 2025; date of current version 14 April 2025. This work was supported in part by the BK21 FOUR Program of the Education and Research Program for Future ICT Pioneers, Seoul National University, in part by the Seoul National University Electric Power Research Institute, and in part by the National Research Foundation of Korea (NRF) grant funded by the Korea Government (MSIT) (RS-2024-00354687). Recommended for publication by Associate Editor A. M. Trzynadlowski. *(Corresponding author: Jung-Ik Ha.)*

The authors are with the Department of Electrical and Computer Engineering, Seoul National University, Seoul 08826, South Korea (e-mail: wronskian@snu.ac.kr; babypighill0@snu.ac.kr; jungikha@snu.ac.kr).

Color versions of one or more figures in this article are available at https://doi.org/10.1109/TPEL.2025.3546298.

Digital Object Identifier 10.1109/TPEL.2025.3546298

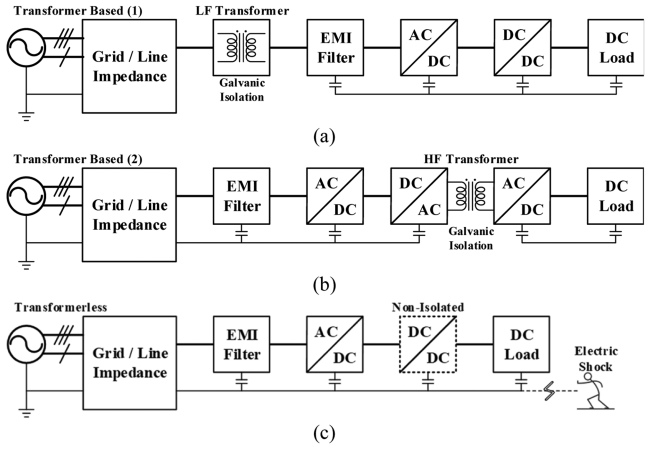

Fig. 1. System diagram of AC–DC power conversion system. (a) LF transformer. (b) HF transformer. (c) Transformerless.

The ac–dc power converter is composed of differential-mode (DM) and common-mode (CM) components. The DM component is defined as a differential voltage and current at each port of the converter, determining the power transfer of the system. In contrast, the CM component is defined as a sum of the voltage and current at each port, which does not contribute to power transfer. The CM voltage (CMV) of the system induces a CM circulating current, which flows into the ground and along the surface of the device through parasitic components or radiates as electromagnetic waves, forming a CM closed-loop circuit. Since the CM component generates additional losses, it deteriorates the system performance.

To mitigate the effect of CMV, a galvanic isolation is used in the ac–dc power conversion system. The magnetic-based isolation is typically achieved using a transformer, which has a high CM impedance. Fig. 1(a) and (b) shows the isolated ac–dc power conversion system featuring two-stage ac–dc power conversion with a low-frequency (LF) or high-frequency (HF) transformer. Significantly, the HF transformer-based system is adopted in the EV charging application due to the power density. Since the power consumption has increased in recent years, there is a growing need for higher power density. Accordingly, the transformerless ac–dc power conversion system is emerging as a new paradigm in various applications, including the EV charging

system [4], grid interface converter [5], and portable device [6]. As illustrated in Fig. 1(c), the transformer is eliminated, which accounts for most of the loss and volume. Instead, a nonisolated dc–dc converter or only single-stage ac–dc power conversion is utilized. However, without the isolation barrier, the CMV is no longer blocked, resulting in a CM current, which is called as leakage current. The leakage current presents a critical challenge in industrial applications. As the leakage current flows into the ground loop, a touch current (TC) is generated, which compromises the human safety [7], [8]. Moreover, the HF CM components interfere with other circuits and devices through the parasitic coupling or conduction, causing electromagnetic interference (EMI) issues [9], [10].

To address the challenge of the transformerless converter, the leakage current suppression methods have been studied in recent years. The key objective is to mitigate the impact of the CMV, including both LF components generated by the ac grid, and HF components generated by the switching of the power converter. Research on suppressing the LF leakage currents has been actively pursued in recent years [11], [12], [13], [14], [15], [16], [17], [18], [19], [20], [21]. In these methods, the LF CMV is injected using the power converter to compensate for the CMV created by the ac grid. However, it is challenging to identify an exact value of the grid frequency CMV due to the variations in grid types and grounding methods across different systems. Therefore, the reference of the LF CMV is derived by controlling other system elements. The first approach focuses on controlling the LF CM components of the dc-link voltage to zero, proposed for the single-phase [11] and three-phase converters [12]. These methods involve measuring the voltage difference between the dc-link port and ground port, and reducing the ac component of the measured voltage to zero. The output of the controller is a LF CMV injected by the power converter, suppressing the leakage currents. However, these methods require an exact voltage of the utility ground, which is usually difficult to obtain in practical applications. In actual ac grid, the ground impedance exists and is determined by the grounding method, resulting in a voltage difference between the ground port and the actual utility ground [4]. To resolve this issue, an alternative method connects the ground port directly to the neutral point of the dc-link and controls the neutral voltage to a constant value, as presented for the single-phase [13] and the three-phase ac–dc converters [14]. While effective under the balanced ac grid conditions, these methods are less applicable in practical systems where the grid voltage fluctuations are common. The next approach involves reversely injecting the grid frequency CMV through the feedforward compensation in the single-phase [15], [16], and the three-phase ac–dc converters [17], [18]. Despite their potential, these methods face challenges in accurately identifying the grid frequency CMV. Moreover, the feedforward methods only account for the CM effect from the ac grid and ignore other components such as filter imbalance. To overcome the limitations of voltage-based control methods, a current-based approach is adopted, where the leakage current is directly measured and utilized as a control parameter. Since the leakage current flowing into the ground is directly linked to safety concerns, suppressing it to zero is an effective way to ensure a compliance with safety standards. In addition, the current-based control methods do not rely on the grid type or grounding method information. Several studies have explored the current-based control methods for various transformerless converter, including three-phase back-to-back converter [19], voltage source converter [20], and current source converter [21]. However, existing methods are only analyzed and designed for three-phase grid-connected system. Moreover, these methods are valid only for a balanced three-phase ac grid, neglecting the effect of grid voltage fluctuation and filter imbalance. As a result, proper modeling of the CM plant and precise design of the current-based controller are essential to achieve an effective leakage current suppression in the tranformerless power conversion system.

Meanwhile, the HF CMV is generated by the switching of the pulsewidth modulation (PWM) converters, resulting in HF leakage currents. The mitigation methods of the HF leakage currents have been studied using the passive or active circuit and modified PWM of the power converters [22], [23], [24], [25], [26], [27], [28], [29], [30], [31], [32], [33], [34]. For the grid-connected converter, both DM and CM EMI filters are utilized using the LCL structure. Using a CM transformer, a passive suppression method for HF leakage currents is proposed [22]. However, the passive circuit is bulky, deteriorating the power density of the system. The reconfigurable EMI filter is introduced using the active bi-directional power switches for the single-phase [23] and three-phase ac–dc converters [24]. However, the EMI filter loss is increased significantly as much as the loss generated by the power circuit. An additional leg of the power converter is utilized for the active filtering in the single-phase [25] and three-phase PWM converters [26], remaining the challenges of additional loss, volume, and cost. To overcome the issue of the passive suppression methods, a modified PWM method is a favorable solution, since an additional circuit is not required. For the single-phase PWM converter, a bipolar PWM is commonly used as it has zero instantaneous CMV, excluding the dead-time effect [27]. However, bipolar PWM suffers from high current ripple and losses, so it is often combined with unipolar PWM to reduce leakage currents [28]. Moreover, the bipolar PWM is extended in the two-phase conduction mode in the three-phase topology for the CMV elimination [29]. In three-phase PWM converters operating in three-phase conduction mode, the instantaneous CMV has a nonzero value. Since a zero-state voltage vector contains a large CMV, the reduced-CMV PWM methods exclude the zero vector during the voltage synthesis. For example, in active zero-state PWM (AZSPWM), the zero-state vector is replaced by two opposing active vectors with equal duration [30]. In near-state PWM (NSPWM), only three active voltage vectors are utilized in a switching period to attenuate the HF CMV [31]. The reduced-CMV PWM is combined with the conventional PWM method to reduce losses in two-level [32] and three-level PWM converters [33]. In addition, the HF CMV can be eliminated by using only a medium vector in the three-level PWM converter [34]. However, the existing reduced-CMV PWM methods are applicable only when the LF CMV, or the average CMV remains a degree of freedom. In the transformerless PWM converter, the CMV reference of the power converter is utilized to suppress the

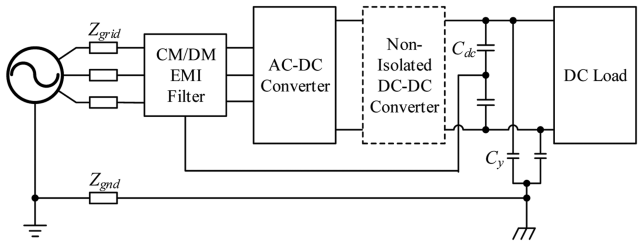

Fig. 2. Transformerless single-stage or two-stage AC–DC power conversion system with EMI filter.

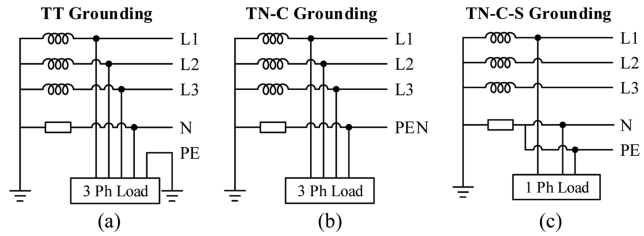

Fig. 3. Representative wiring and grounding system of grid-connected equipment. (a) TT grounding with three-phase load. (b) TN-C grounding with three-phase load. (c) TN-C-S grounding with single-phase load.

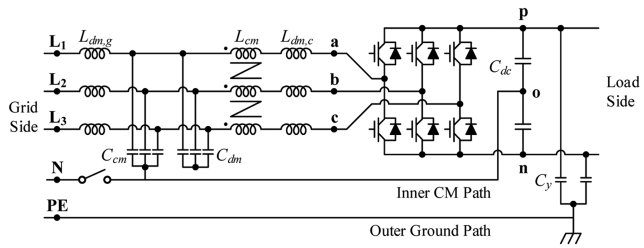

Fig. 4. Configuration of DM and CM EMI filter for grid-connected three-phase PWM converter system.

LF leakage current. As a result, a new PWM method is required to attenuate the HF CMV regardless of the average CMV.

This article proposes the control and modulation methods for suppressing both low- and HF leakage currents in the single-/three-phase transformerless ac–dc converter. Through a comprehensive analysis of the CMV sources, a CM equivalent circuit is developed, considering the filter structure and the grounding system of the grid-connected converter. Based on the derived circuit, a CMV controller is designed to reduce the LF leakage currents, which generates the LF CMV of the PWM converter as an output. The proposed controller utilizes direct measurement of the leakage current as a feedback. Subsequently, a voltage modulation method of the single-/three-phase PWM converter is presented to mitigate the HF leakage currents. The proposed PWM synthesizes the CMV reference of the PWM converter with minimized HF CMV ripple. At last, the proposed methods are verified by an experimental setup of grid-connected trasnformerless PWM converter. The effectiveness of the leakage current suppression is confirmed through a TC evaluation in compliance with the International Electrotechnical Commission (IEC) standard.

II. CM Analysis

To clarify the principle behind the generation of the leakage currents, a comprehensive analysis of the CM component is conducted. Considering the structure of the EMI filter and the grounding system, a practical CM equivalent circuit is derived, which is fundamental to the system plant for the CMV control.

A. Configuration of AC–DC Power Conversion System

Fig. 2 illustrates a transformerless ac–dc power conversion system, featuring either a single or two-stage power converter along with an EMI filter. For the ac–dc power conversion, a single-phase or three-phase ac–dc converter such as a PWM converter is employed. An optional nonisolated type dc–dc converter is added to operate across a wide load range and to mitigate power fluctuations. The connection between the ac grid and the power conversion system, which is influenced by the wiring and grounding system, is depicted in Fig. 3 [35]. In Fig. 3(a) and (b), three-phase equipment is connected to the ac grid using TT and TN-C grounding systems. The power wire of the equipment is connected to L1, L2, L3 ports, while the neutral (N) and protective earth (PE) ports are selectively connected according to the grounding system. In the TT grounding, the neutral of the ac grid is connected while the equipment is grounded locally, resulting in significant ground impedance, Z_{gnd}, due to the disparities between the local ground and the utility ground. In the TN-C grounding, the ground of the equipment is directly connected to the PEN port, which serves as both the neutral and earth of the ac grid simultaneously. Fig. 3(c) shows the single-phase equipment connected to the ac grid with the TN-C-S grounding method, where the power port is connected to L and N, and the ground port is connected to PE, which is merged with N.

To ensure the electromagnetic compatibility of the grid-connected converter, an EMI filter consisting of DM filter and CM filter is designed. A simple third-order *LCL*-type filter is applied for DM attenuation, as shown in Fig. 4. For the CM filter, a CM choke is installed in front of the power converter, and half of the DM inductance is also utilized. The neutral point of the CM capacitor is linked to the neutral point of the dc-link, establishing an internal CM path, which is optionally connected to the N port. This configuration, referred to as a floating EMI filter, effectively attenuates the HF CMV generated by the PWM switching of power converter [4]. Furthermore, a Y-capacitor, typically less than 500 nF including parasitic components, is connected between the dc-link and the external ground path linked to the PE port. In some previous studies, the neutral point of the dc port is directly grounded with a low resistance [13], [14], [19], [21]. While this approach simplifies the plant analysis by neglecting the parasitic capacitance, it is impractical in the actual system. In the grid-connected converter system, the Y-capacitance is placed between the ground and the load, and its value is determined by the system design and cannot be easily adjusted [3], [4], [9]. As a result, a proper modeling of the CM plant is essential to achieve effective leakage current suppression in the transformerless power conversion system.

B. Source of CMV

The sources of the CMV in the ac–dc power conversion system can be divided into LF and HF sources. The ac grid generates CMV with the grid fundamental and harmonic frequencies. Depending on the grounding system, the PE wire is connected to the utility ground (TN-S), the neutral point of the grid (TN-C), or the local ground (TT). Accordingly, the grid frequency CMV, $v_{g,\mathrm{cm}}$ is generated depending on the system configuration, which is expressed as

$$v_{g,\mathrm{cm}} = \frac{\sum_{k=1}^{n_{ph}} v_{Lk}}{n_{ph}} \tag{1}$$

where v_{Lk} denotes the voltage at the power port referenced to the ground and n_{ph} denotes the number of phases. In a three-phase TT grounded system, the grid frequency CMV is ideally zero if the grid voltage is balanced. However, the variations in the grid voltage, such as harmonics, sags, and fluctuations, contribute to CMV. In the single-phase TN-C-S grounded system, the grid frequency CMV is approximately half of the grid voltage. In addition, the imbalance in grid impedance and the EMI filter can become another source of CMV during power delivery, generating the LF leakage currents which flow into the outer ground loop.

Meanwhile, the HF CMV is generated by the PWM switching of the ac–dc and dc–dc power converter. In the PWM converter illustrated in Fig. 4, the switching state of each phase determines the switching frequency CMV, $v_{\mathrm{conv,cm}}$, which is derived as

$$v_{\mathrm{conv,cm}} = \begin{cases} \frac{v_{ao}+v_{bo}}{2} & \text{(single phase)} \\ \frac{v_{ao}+v_{bo}+v_{co}}{3} & \text{(three phase)} \end{cases} \tag{2}$$

where v_{ao}, v_{bo}, v_{co} represent the instantaneous voltage of each phase referenced to the neutral point of the dc-link. Since the switching state determines the instantaneous CMV, the pattern of the HF CMV depends on the PWM method employed by the PWM converter.

C. CM Equivalent Circuit

Using the CMV sources analyzed in the last section, the CM equivalent circuit of ac–dc power conversion system is developed. In Fig. 5(a), the equivalent circuit of a conventional isolated topology is illustrated, featuring an isolation barrier that blocks the CM path. The CM equivalent impedance is calculated as

$$L'_{\mathrm{cm},c} = L_{\mathrm{cm}} + \frac{L_{\mathrm{dm},c}}{n_{\mathrm{ph}}},\quad L'_{\mathrm{cm},g} = \frac{L_{\mathrm{dm},g}}{n_{\mathrm{ph}}}$$
$$C'_{\mathrm{cm}} = n_{\mathrm{ph}}\, C_{\mathrm{cm}},\quad C'_{\mathrm{dc}} = 2C_{\mathrm{dc}},\quad C'_y = 2C_y \tag{3}$$

with the ground impedance determined by the grounding system. In contrast, the equivalent circuit for a nonisolated topology is described in Fig. 5(b), where a closed-loop CM path is created. The floating filter structure allows the HF leakage currents generated by the power converter to flow into the inner loop and be attenuated by the EMI filter. However, the LF leakage currents, induced by the ac grid, flow directly into the external ground loop without any attenuation.

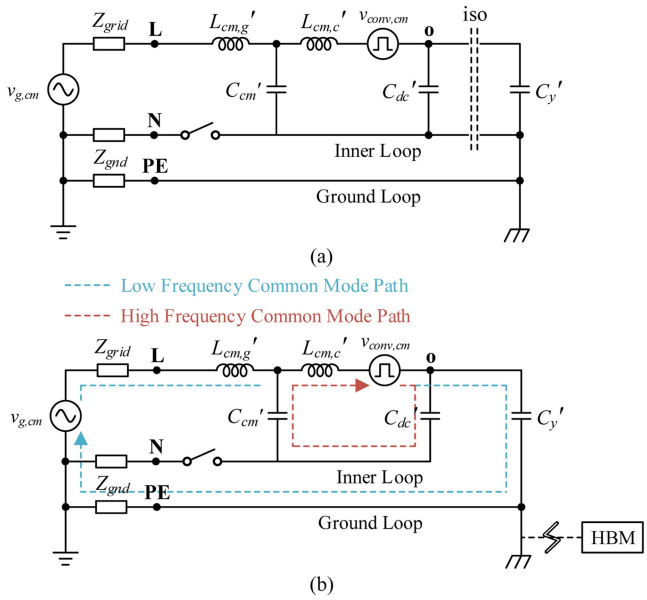

Fig. 5. CM equivalent circuit of AC–DC power conversion system. (a) Conventional isolated topology. (b) Nonisolated topology with touch condition of human body model.

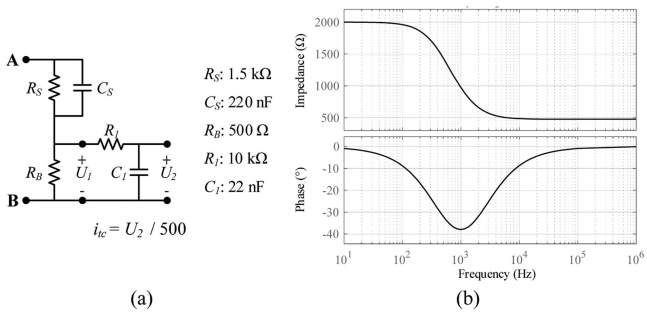

Fig. 6. Human body impedance model in IEC 60990 standard. (a) Impedance model. (b) Bode diagram of impedance model.

To evaluate the human safety of the system, the TC is measured. In scenarios where human contact occurs, the human body is connected with the PE wire, as depicted in Fig. 5(b). The human body impedance model (HBM) is utilized, which follows the IEC 60990 standard, as illustrated in Fig. 6(a) [36]. Since the HBM circuit behaves as a 2000 Ω resistor within the grid frequency band, as shown in Fig. 6(b), the voltage of the PE node induces a TC, i_{tc}, which is derived by the HBM. The PE node voltage is generated by the various CMV sources. The transfer function between the CMV sources, v_{cm}, and PE node voltage, v_{PE}, is expressed as

$$\frac{v_{\mathrm{PE}}}{v_{\mathrm{cm}}} = \frac{Z_{\mathrm{gnd}}}{\frac{1}{sC'_y} + sL'_{\mathrm{cm},g} + Z_{\mathrm{gnd}}} \frac{Z_{\mathrm{filt}}}{sL'_{\mathrm{cm},c} + Z_{\mathrm{filt}}}$$
$$\text{where } Z_{\mathrm{filt}} = \left(\frac{1}{sC'_{\mathrm{dc}}} + \frac{1}{sC'_{\mathrm{cm}}}\right) \parallel \left(\frac{1}{sC'_y} + sL'_{\mathrm{cm},g} + Z_{\mathrm{gnd}}\right) \tag{4}$$

with the corresponding bode diagram illustrated in Fig. 7. Notably, the parameters contain information about the number of

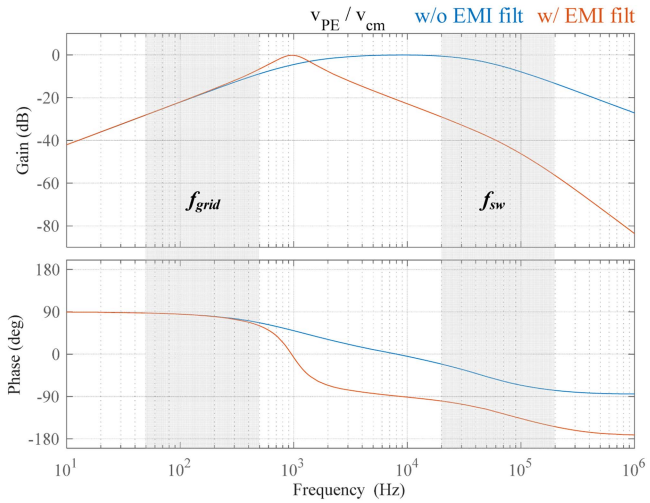

Fig. 7. Bode diagram of transfer function between CMV source and leakage current flowing into PE wire.

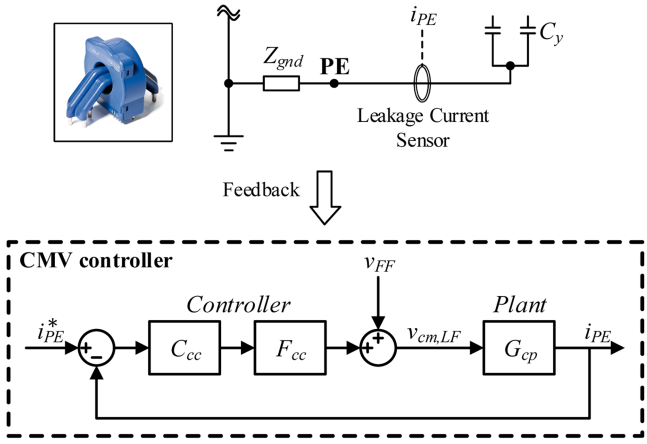

Fig. 8. System diagram of proposed CMV controller with leakage current sensor.

phases $n_{\text{ph}}$and the Y-capacitance C_y. While the HF CMV generated by the switching of the converter is effectively attenuated by the EMI filter, the impact of the LF CMV created by the ac grid remains a concern. Due to the critical role of LF CMV in generating leakage currents, it is essential to employ an active control method to mitigate its effect.

III. Proposed CMV Control

To suppress the LF leakage currents, this paper proposes a control method of the CMV in the ac–dc converter, such as a PWM converter. Since the CMV within the converter does not participate in the power delivery, it is utilized to mitigate the effect of grid frequency CMV. Utilizing the HF CMV generated by the power converter, a LF CMV is injected into the system through an averaging.

A. Controller Design

The LF leakage currents primarily flow into the PE wire, as shown in Fig. 5(b). The magnitude of the leakage currents is relatively small, on the order of mA, and is directly influenced by the grid frequency CMV. Moreover, the leakage currents are susceptible to the grid harmonics, since the higher harmonic components are less attenuated, as described in Fig. 7. To ensure the safety of the system, the LF leakage currents are suppressed by the proposed CMV control method, regardless of the phase and grounding system of the ac grid. The leakage current flowing into the PE wire, i_{PE}, is directly measured by a leakage current sensor and employed for a feedback, as illustrated in Fig. 8. The proposed controller is briefly introduced for the single-phase ac–dc converter in the prepresented research [37]. In this article, an improved design method of the controller is provided and extended for both single-phase and three-phase applications.

The design of the proposed CMV controller begins with deriving the plant model using the CM equivalent circuit. Using the LF CM path shown in Fig. 5(b), a transfer function between the LF leakage current flowing into the PE wire, $i_{\text{PE,LF}}$, and the LF CMV produced by the power converter, $v_{\text{cm,LF}}$, is expressed as

$$G_{\text{cp,LF}}(s) = \frac{i_{\text{PE,LF}}}{v_{\text{cm,LF}}} = \frac{1}{sL'_{\text{cm}} + \frac{1}{sC'_y} + Z_{\text{grid}} + Z_{\text{gnd}}}$$

$$\text{where } L'_{\text{cm}} = L'_{\text{cm},c} + L'_{\text{cm},g}. \tag{5}$$

Employing the derived plant model, the leakage current feedback-based CMV controller is designed. The proposed controller features a two-stage cascaded structure. The first stage involves formulating a plant model compensator, $C_{\text{cc}}(s)$, as a system with one pole and two zeros, represented by

$$C_{\text{cc}}(s) = \frac{1}{G_{\text{cp,LF}}(s)} = k_p + \frac{k_i}{s} + sk_d \tag{6}$$

where k_p, k_i, and k_d are the gains of PID structured system. The system gain is derived using the inverse of the LF plant model, which is calculated as

$$\begin{aligned} k_p &= R_{\text{grid}} + R_{\text{gnd}}, \\ k_i &= C'_y, \\ k_d &= L'_{\text{cm}} + L_{\text{grid}} + L_{\text{gnd}} \cong L'_{\text{cm}}. \end{aligned} \tag{7}$$

Since the plant model compensator sets the open-loop transfer function to unity, a function shaper, $F_{\text{cc}}(s)$, is designed to shape the closed-loop transfer function of the controller. Given that the leakage currents exhibit a pure ac waveform with grid fundamental and harmonic frequency, the design method of the controller considers two primary conditions: a negative infinite dc gain and a near unity gain at the grid fundamental and harmonic frequency. In order to satisfy these criteria, a parallel resonant controller is utilized, which is expressed as

$$F_{\text{cc}}(s) = \sum_{k=1}^{2n-1} \frac{2k_r\omega_{\text{rc}}s}{s^2 + 2\omega_{\text{rc}}s + \omega_{\text{rk}}^2} \tag{8}$$

where ω_{rk} represents the resonant frequency, which is set as the fundamental and harmonic frequencies of the ac grid, ω_{rc} the damping frequency, and k_r the gain of the resonant controller.

As described in Fig. 8, the overall CMV controller is constructed from a product of the plant model compensator and the function shaper. In addition, a voltage feedforward is optionally incorporated to enhance transient response. If the grounding system and the precise value of the CMV generated by the ac grid are known, the voltage feedforward is added as the CMV in (1). In contrast, when the grid frequency CMV is unidentifiable in a practical system, the voltage feedforward is applied to compensate for the plant model at the frequency band lower than the grid frequency, which is expressed as

$$v_{\mathrm{FF}}\ (s) = \frac{1}{sC'_y}\ i_{\mathrm{PE}} \tag{9}$$

since the Y-capacitance is predominant at the LF. Consequently, the proposed CMV control method attenuates the LF leakage currents in both single-phase and three-phase ac grid-connected power conversion systems.

B. Performance and Stability Analysis

To assess the performance of the proposed CMV controller, the transfer function of the control loop is derived as

$$\begin{aligned} G_{\mathrm{cc,ol}}\ (s) &= C_{\mathrm{cc}}\ (s)\, F_{\mathrm{cc}}\ (s)\, G_{\mathrm{cp}}\ (s) \\ G_{\mathrm{cc,cl}}\ (s) &= \frac{C_{\mathrm{cc}}\ (s)\, F_{\mathrm{cc}}\ (s)\, G_{\mathrm{cp}}\ (s)}{1 + C_{\mathrm{cc}}\ (s)\, F_{\mathrm{cc}}\ (s)\, G_{\mathrm{cp}}\ (s)} \end{aligned} \tag{10}$$

with the corresponding bode diagram illustrated in Fig. 9(a) and (b). The diagram shows that the closed-loop gain of the controller reaches unity gain with zero phase at the grid fundamental and harmonic frequencies, demonstrating the effectiveness in mitigating the grid frequency CMV. The dc gain approaches negative infinity, indicating strong robustness against the discretization effects in digital control systems. Furthermore, the proposed CMV control method provides comparable closed-loop performance in both single-phase and three-phase systems. When the voltage feedforward is applied, it further improves the transient response of the controller in the LF band, as described by the orange line.

Since the proposed controller is designed to compensate for the LF plant model, it is clear that the controller has an inherent stability in the LF band under ideal conditions. However, it is required to evaluate the stability in the HF band, and the practical condition including the variations in parameters and the time delay introduced by the digital control system. Accordingly, the open-loop transfer function outlined in (10) is reconfigured as

$$\begin{aligned} G_{\mathrm{cc,ol}}\ (s) &= C_{\mathrm{cc}}\ (s)\, F_{\mathrm{cc}}\ (s)\, G_{\mathrm{cp}}\ (s)\, G_d\ (s) \\ &\cong F_{\mathrm{cc,HF}}\ (s)\, G_{\mathrm{cp,HF}}\ (s)\, G_d\ (s) \\ &= \frac{2k_r\omega_{\mathrm{rc}}}{s}\ \frac{1}{s^2 L'_{\mathrm{cm}} C'_{\mathrm{cm}} + s\frac{L'_{\mathrm{cm}}}{R_{\mathrm{gnd}}} + 1}\ \frac{1}{st_d + 1} \end{aligned} \tag{11}$$

where t_d denotes the time delay of the digital control system. To evaluate the stability of the system, the characteristic equation of the controller is calculated as

$$F\ (s) = 1 + F_{\mathrm{cc,HF}}\ (s)\, G_{\mathrm{cp,HF}}\ (s)\, G_d\ (s)\,. \tag{12}$$

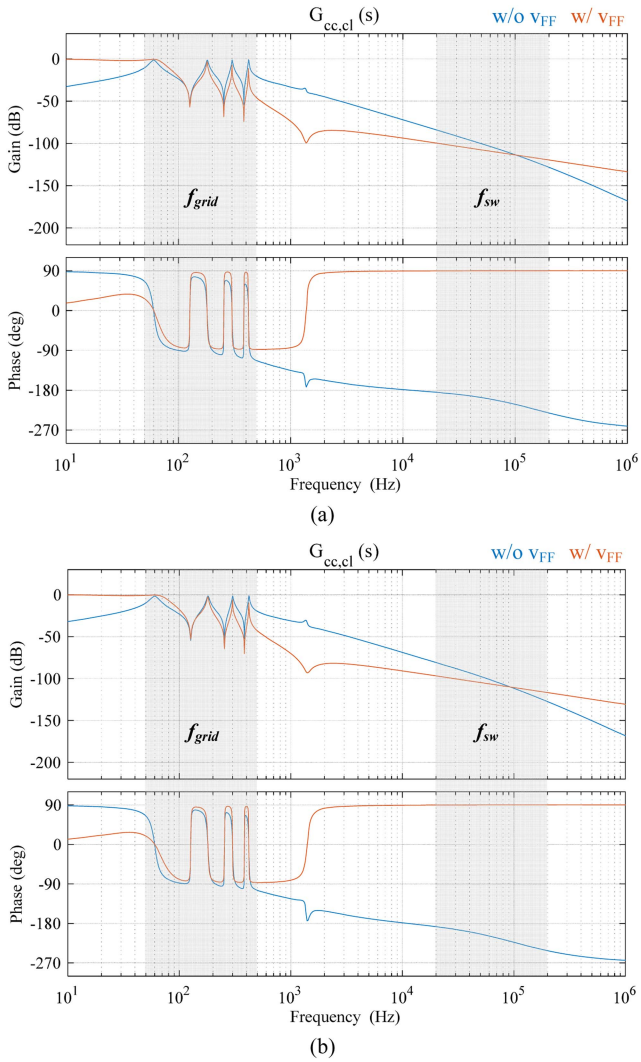

Fig. 9. Bode diagram of closed-loop transfer function of the proposed CMV controller based on leakage current feedback. (a) Single-phase topology. (b) Three-phase topology.

Given that the parameters in (11) maintain positive values, the condition for the control stability is derived as

$$2k_r\omega_{\mathrm{rc}}\left(L'_{\mathrm{cm}}C'_{\mathrm{cm}} + t_d\frac{L'_{\mathrm{cm}}}{R_{\mathrm{gnd}}}\right) < 1 \tag{13}$$

using the Routh-Hurwitz stability criterion. The ratio of k_r and ω_{rc} is adjusted to set the peak magnitude at the resonant frequency. A high ratio of k_r improves the performance and transient response of the controller, while a high ratio of ω_{rc} improves the stability and the robustness against the parameter variation of the plant. Taking these tradeoffs into account, the ratio between the two variables is optimized through a tuning process. The final designed parameters are summarized in Table I. The gain margin at a phase of -180° becomes around 71 dB, verifying the stability of the proposed controller.

The PID gain settings for the plant model compensator are specified in (7). However, the system parameters can change based on the operating condition, particularly the ground impedance and Y-capacitance, which are not easily adjustable.

TABLE I
DESIGNED PARAMETERS OF CONTROLLER

Symbol	Parameter	Nominal Value
k_p	P Gain	100
k_i	I Gain	1×10^{-6}
k_d	D Gain	0.0012
ω_{r1}	Resonant Frequency	$2\pi \times 60$ rad
ω_{rc}	Damping Frequency	$2\pi \times 0.1$ rad
k_r	Resonant Gain	30

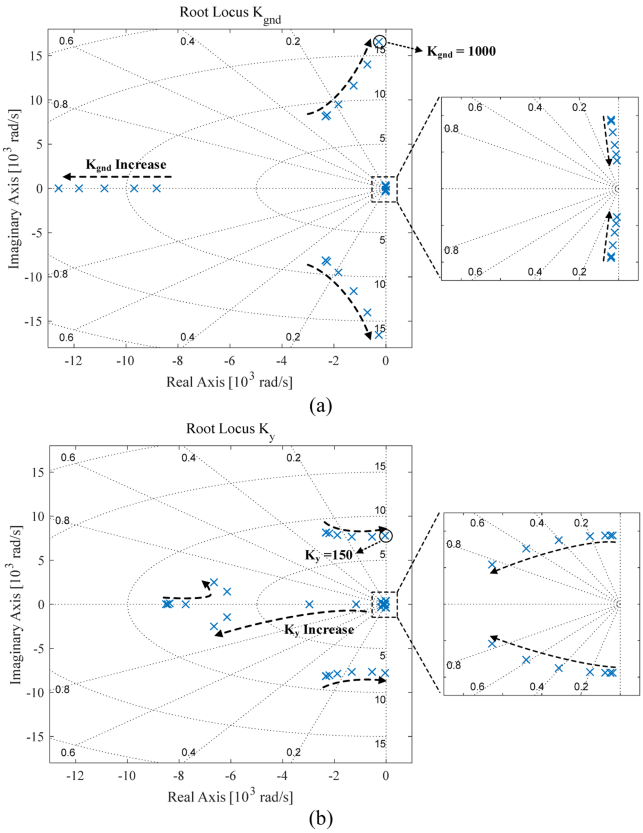

Fig. 10. Root locus of closed-loop controller according to parameter variation. (a) Ground impedance variation from 0.01 to 1000. (b) Y-capacitance variation from 0.01 to 150.

Therefore, the robustness to parameter variation is analyzed using the root locus of the controller, as described in Fig. 10. The coefficient of the parameter variation is defined as

$$K_{\text{gnd}} = \frac{\hat{R}_{\text{gnd}}}{R_{\text{gnd}}}, \quad K_y = \frac{\hat{C}_y}{C_y} \tag{14}$$

where the superscript ^ denotes an estimated value utilized for the gain scheduling. As shown in Fig. 10(a), the system pole remains in the left half-plane until when the ground impedance variation reaches up to 1000 times its actual value. In addition, the system maintains stability even when the Y-capacitance increases up to 150 times its original value, as depicted in Fig. 10(b). This analysis indicates that despite the susceptibility of certain parameters to the fluctuations, the proposed CMV

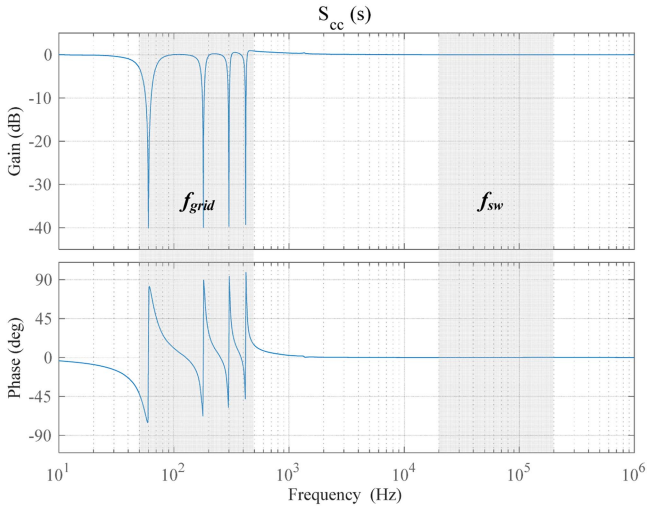

Fig. 11. Bode diagram of sensitivity function of proposed CMV controller.

controller achieves a significant robustness against the parameter variations.

To evaluate the tracking performance under the parameter variation, the sensitivity function $S_{\text{cc}}(s)$ of the closed-loop controller is given by

$$\begin{aligned} S_{\text{cc}}(s) &= \frac{\partial G_{\text{cc,cl}}(s)/G_{\text{cc,cl}}(s)}{\partial G_{\text{cp}}(s)/G_{\text{cp}}(s)} \\ &= \frac{1}{1 + C_{\text{cc}}(s) F_{\text{cc}}(s) G_{\text{cp}}(s)} \end{aligned} \tag{15}$$

which indicates the change in the transfer function in response to changes in the plant parameters. For a sinusoidal reference or disturbance, minimizing the magnitude of the sensitivity function improves the tracking performance of the resonant controller [38], [39]. The bode diagram in Fig. 11 shows the magnitude of the sensitivity function, revealing a low value of around -40 dB at the grid fundamental and harmonic frequencies. This confirms the robustness of the proposed CMV control method, particularly in rejecting disturbances at the target frequencies.

C. Implementation Issues

The proposed CMV controller employs direct measurement of the leakage current, which is readily available in the practical grid-connected power conversion systems. In the industrial applications, the CM leakage current is typically measured to detect the ground faults and to trigger the ground fault circuit interrupter [40], [41].

Recently, a leakage current sensor with analog feedback has been developed for grid-connected equipment, offering high bandwidth and resolution [41]. This leakage current sensor serves both as a measurement tool for leakage current and as a ground fault detection device. Consequently, the proposed CMV control method incurs no additional cost beyond the existing leakage current sensor, making it fully applicable to industrial systems.

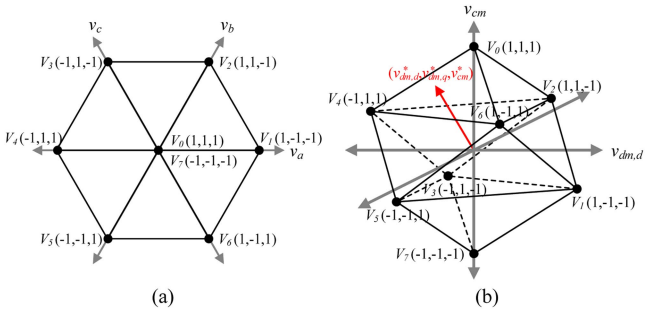

Fig. 12. Space vector diagram for three-phase PWM converter. (a) Conventional PWM. (b) Proposed HDSVPWM.

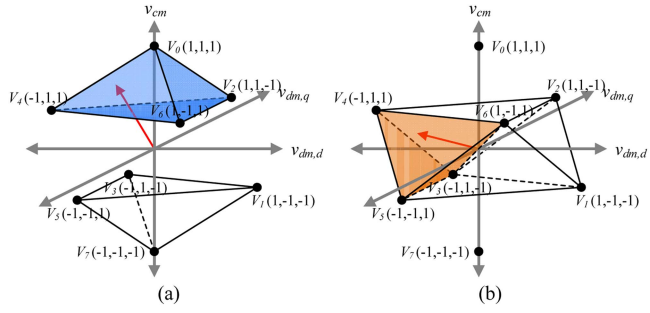

Fig. 13. Space vector region of proposed three-phase HDSVPWM. (a) High CMV region. (b) Low CMV region.

TABLE II
VOLTAGE VECTORS OF THREE-PHASE PWM

Vector	Switching State	Common Mode Voltage
V_0	(1, 1, 1)	$v_{dc}/2$
V_1	(1, -1, -1)	$-v_{dc}/6$
V_2	(1, 1, -1)	$v_{dc}/6$
V_3	(-1, 1, -1)	$-v_{dc}/6$
V_4	(-1, 1, 1)	$v_{dc}/6$
V_5	(-1, -1, 1)	$-v_{dc}/6$
V_6	(1, -1, 1)	$v_{dc}/6$
V_7	(-1, -1, -1)	$-v_{dc}/2$

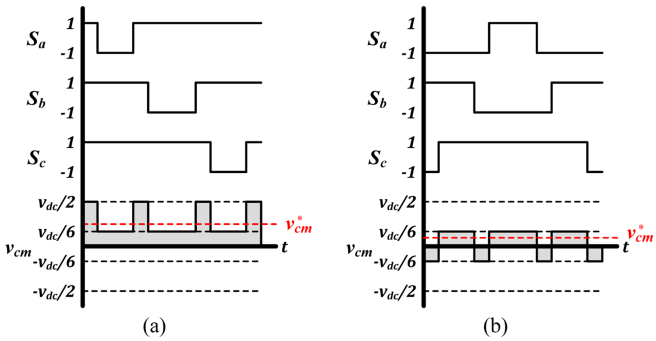

Fig. 14. Switching state and instantaneous CMV of three-phase HDSVPWM. (a) High CMV region. (b) Low CMV region.

IV. PROPOSED PWM

The output of the proposed CMV controller is the CMV reference for the PWM converter. In the conventional ac–dc power conversion system, the differential-mode voltage (DMV) reference is related to the power delivery. In contrast, the average CMV, commonly referred to as a zero-sequence voltage, remains a degree of freedom. For example, in the AZSPWM, the average CMV is determined by the duration of odd and even voltage vectors, without additional adjustability. In the remote-state PWM (RSPWM) for the three-phase PWM converter, the average CMV is fixed at $v_{\rm dc}/6$ or $-v_{\rm dc}/6$ [30]. In the bipolar PWM for the single-phase PWM converter, the instantaneous CMV is always zero, naturally, the average CMV is also zero.

However, in the proposed transformerless PWM converter, the CMV reference is set to a specific value by the proposed CMV controller. Given the previous reduced-CMV PWM methods are only effective when the LF CMV is either zero or predefined by PWM sequence, a new PWM method is necessary to synthesize both the CMV and DMV references simultaneously. This article introduces PWM methods for both three-phase and single-phase applications based on a uniform principle.

A. Three-Phase PWM for Leakage Current Suppression

The voltage generated by the PWM converter is divided into the DMV, $v_{\rm dm}$, for the power conversion and the CMV, $v_{\rm cm}$, for the leakage current suppression. In the conventional space vector PWM (SVPWM) of three-phase PWM converter, a space vector diagram is employed to synthesize the voltage reference using an *abc* axis representation, as depicted in Fig. 12(a) and [29]. The diagram features eight voltage vectors, V_{0-7}, indicated by dots, with the switching state of phase *abc* denoted as 1 for the upper side and -1 for the lower side, as outlined in Table II. In the conventional PWM, the *abc* axis visualizes the DMV of each voltage vector. However, the CMV is not represented in the space vector region, as it is independent of the DMV. To address this limitation, a high-dimensional space vector PWM (HDSVPWM) is proposed for the three-phase PWM converters. The proposed PWM extends the conventional PWM by applying the *dq* reference of the stationary reference frame along the *x*-axis and *y*-axis, while the CMV reference is applied along the *z*-axis of the spatial space vector diagram, as described in Fig. 12(b). Therefore, the dimension of the space vector region is increased to three. This approach allows the DMV and CMV references to be simultaneously represented as a single vector, expressed as

$$\vec{v}_{\rm conv} = {v_{{\rm dm},d}}^* \, \mathbf{i} + {v_{{\rm dm},q}}^* \mathbf{j} + {v_{\rm cm}}^* \mathbf{k} \tag{16}$$

where the superscript $*$ denotes a reference value, $v_{{\rm dm},d}$ and $v_{{\rm dm},q}$ each denotes the *dq* reference of DMV at the stationary reference frame. To synthesize the reference vector, the type and duration of the voltage vectors are determined. Each voltage vector has its unique value of the CMV and DMV, represented as a point in the spatial coordinate system. Since the reference value has three types of voltage in (16) and the sum of each voltage vector's duration equates to a switching period, at least four types of voltage vectors are necessary to create the reference vector. Furthermore, it is advantageous to utilize only minimum voltage vectors to reduce the switching loss. As a result, the reference voltage vector is synthesized using four adjacent voltage vectors,

TABLE III
VOLTAGE VECTORS OF SINGLE PHASE PWM

Vector	Switching State	Common Mode Voltage
V_1	(1, -1)	0
V_2	(1, 1)	$v_{dc}/2$
V_3	(-1, 1)	0
V_4	(-1, -1)	$-v_{dc}/2$

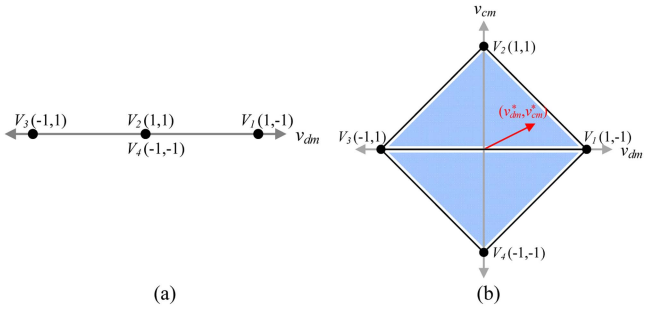

Fig. 15. Space vector diagram for single-phase PWM converter. (a) Conventional PWM. (b) Proposed HDSVPWM.

represented as a tetrahedron in the spatial coordinate system. The detailed derivation process is provided in the Appendix.

Various scenarios are considered for selecting four among the eight available voltage vectors for synthesis. As shown in Table II, the pattern of instantaneous CMV depends on the selected voltage vectors, where $v_{\rm dc}$ represents the dc-link voltage. To mitigate the leakage currents, the voltage vectors are selected to minimize the HF CMV ripple. In the proposed three-phase HDSVPWM, the magnitude of the CMV is expressed by the z-coordinate. Accordingly, the four vectors are selected with the smallest difference in the z-coordinate, and the space vector region is subdivided along the z-axis, as described by the tetrahedron in Fig. 13. The space vector region is classified into two types according to the magnitude of the CMV reference. If the CMV reference is larger than $v_{\rm dc}/6$, the upper tetrahedron is utilized, where the instantaneous CMV of the voltage vectors is $v_{\rm dc}/2$ and $v_{\rm dc}/6$. For instance, in the case of the reference vector shown in Fig. 13(a), the duration of each voltage vector is derived as

$$
\begin{aligned}
t_{V0} &= \frac{-v_{\rm dc}+6v^*_{\rm cm}}{2v_{\rm dc}}\, t_{\rm sw},\\
t_{V2} &= \frac{v_{\rm dc}+v^*_{{\rm dm},d}+\sqrt{3}v^*_{{\rm dm},q}-2v^*_{\rm cm}}{2v_{\rm dc}}\, t_{\rm sw},\\
t_{V4} &= \frac{v_{\rm dc}-2v^*_{{\rm dm},d}-2v^*_{\rm cm}}{2v_{\rm dc}}\, t_{\rm sw},\\
t_{V6} &= \frac{v_{\rm dc}+v^*_{{\rm dm},d}-\sqrt{3}v^*_{{\rm dm},q}-2v^*_{\rm cm}}{2v_{\rm dc}}\, t_{\rm sw}
\end{aligned}
\tag{17}
$$

where t_V denotes a duration of voltage vector and $t_{\rm sw}$ denotes a switching period. Meanwhile, the middle tetrahedron is utilized when the CMV reference is smaller than $v_{\rm dc}/6$ and larger than $-v_{\rm dc}/6$. One of the six tetrahedrons is selected for voltage

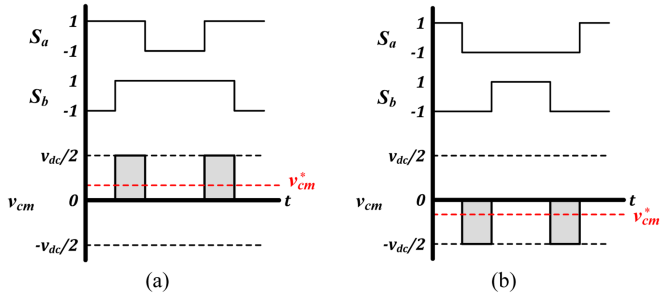

Fig. 16. Switching state and instantaneous CMV of single-phase HDSVPWM. (a) Positive CMV. (b) Negative CMV.

synthesis, where the instantaneous CMV of voltage vectors is $\pm v_{\rm dc}/6$. In the case of the reference vector shown in Fig. 13(b), the duration of each voltage vector is derived as

$$
\begin{aligned}
t_{V3} &= \frac{v_{\rm dc}+v^*_{{\rm dm},d}+\sqrt{3}v^*_{{\rm dm},q}-2v^*_{\rm cm}}{2v_{\rm dc}}\, t_{\rm sw}\; t_{V4}\\
&= \frac{-2v^*_{{\rm dm},d}+4v^*_{\rm cm}}{2v_{\rm dc}}\, t_{\rm sw}\; t_{V5}\\
&= \frac{-v^*_{{\rm dm},d}-\sqrt{3}v^*_{{\rm dm},q}-4v^*_{\rm cm}}{2v_{\rm dc}}\, t_{\rm sw}\; t_{V6}\\
&= \frac{v_{\rm dc}+2v^*_{{\rm dm},d}+2v^*_{\rm cm}}{2v_{\rm dc}}\, t_{\rm sw}.
\end{aligned}
\tag{18}
$$

The switching state and the instantaneous CMV of the proposed three-phase HDSVPWM are illustrated in Fig. 14. At the high CMV region in Fig. 14(a), only the voltage vector with a positive CMV is utilized. In contrast, at the low CMV region in Fig. 14(b), only the voltage vector with a lower magnitude of CMV is utilized. Since the CMV level of each switching state is limited to only two, the proposed PWM method minimizes the HF CMV ripple, resulting in the suppression of the HF leakage current.

B. Single-Phase PWM for Leakage Current Suppression

In the single-phase PWM converter, the voltage vector and its switching state are defined in Table III. Due to the reduced number of the voltage vectors, there are fewer variations of the PWM methods. When the CMV reference is zero, the voltage vector with zero instantaneous CMV is only utilized, which corresponds to the conventional bipolar PWM. Therefore, the conventional space vector diagram of the single-phase PWM converter is simplified to a single line, as shown in Fig. 15(a). However, when the proposed CMV control method is applied, the CMV and DMV references are generated independently. To address this issue, the single-phase HDSVPWM is proposed, which extends the conventional PWM by applying the DMV reference along the x-axis, while the CMV reference is applied along the y-axis of the space vector diagram, as described in Fig. 15(b). Therefore, the dimension of the space vector region is increased to two. As described in Fig. 15(b), the voltage reference is represented as a single vector in a two-dimensional

(a) (b)

Fig. 17. Experiment setup. (a) Single-phase and three-phase compatible PWM converter. (b) Human body impedance model.

space vector diagram, expressed as

$$\vec{v}_{\text{conv}} = v^*_{\text{dm}}\,\mathbf{i} + v^*_{\text{cm}}\mathbf{j} \tag{19}$$

where v^*_{dm} denotes the DMV reference. Similar to the case of three-phase PWM, the reference vector is synthesized using three voltage vectors, creating a triangular space vector region. The detailed derivation process is provided in the Appendix. To minimize the HF CMV ripple, the space vector region is subdivided along the y-axis as much as possible. For example, when the CMV reference is positive, the upper triangular region is utilized for the voltage synthesis. In this region, the duration of each voltage vector is calculated as

$$\begin{aligned} t_{V1} &= \frac{v_{\text{dc}} + 2v^*_{\text{dm}} - 2v^*_{\text{cm}}}{2v_{\text{dc}}}\, t_{\text{sw}}, \\ t_{V2} &= \frac{2v^*_{\text{cm}}}{v_{\text{dc}}}\, t_{\text{sw}}, \\ t_{V3} &= \frac{v_{\text{dc}} - 2v^*_{\text{dm}} - 2v^*_{\text{cm}}}{2v_{\text{dc}}}\, t_{\text{sw}}. \end{aligned} \tag{20}$$

In contrast, when the CMV reference is negative, the duration of each voltage vector is calculated as

$$\begin{aligned} t_{V1} &= \frac{v_{\text{dc}} + 2v^*_{\text{dm}} + 2v^*_{\text{cm}}}{2v_{\text{dc}}}\, t_{\text{sw}}, \\ t_{V3} &= \frac{v_{\text{dc}} - 2v^*_{\text{dm}} + 2v^*_{\text{cm}}}{2v_{\text{dc}}}\, t_{\text{sw}}, \\ t_{V4} &= -\frac{2v^*_{\text{cm}}}{v_{\text{dc}}} t_{\text{sw}}. \end{aligned} \tag{21}$$

Fig. 16 illustrates the switching state and instantaneous CMV of the single-phase HDSVPWM for both positive and negative CMV. As shown in the figure, the CMV level is restricted to only two values, effectively minimizing the HF CMV ripple. As a result, the proposed single-phase and three-phase HDSVPWM methods significantly reduce the HF CMV ripple and leakage currents in the transformerless PWM converters, regardless of the CMV and DMV references. Furthermore, the principle of the proposed PWM method can be extended to the multilevel converters.

In the reduced-CMV PWM methods, the dead-time effect is a critical issue, generating an unintended CMV spike [42]. The CMV spikes occur when the switching state changes, but the instantaneous CMV remains constant. Specifically, this occurs at the simultaneous switching of two different legs [43]. However, in the proposed single-phase and three-phase HDSVPWM methods illustrated in Figs. 14 and 16, there are no pulse patterns where the switching instants of the two phases overlap. Therefore, the proposed HDSVPWM naturally mitigates the dead-time effect on the CMV spikes.

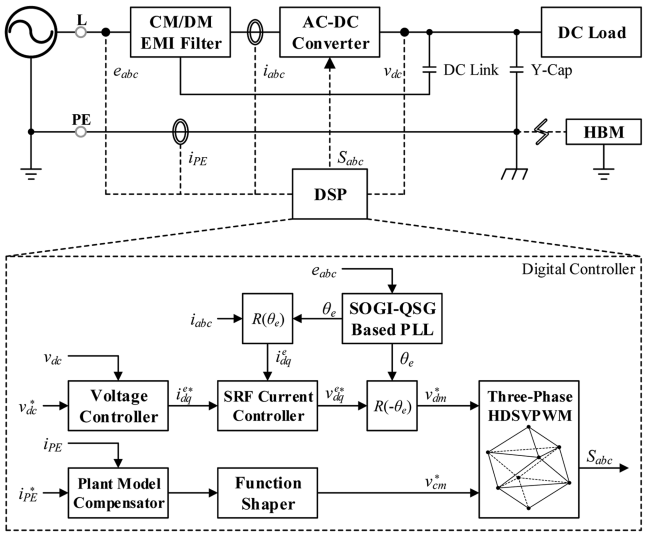

Fig. 18. Overall system diagram for proposed control and modulation methods of single-/three-phase PWM converter.

V. Simulation and Experimental Verification

To validate the effectiveness of the proposed control and modulation methods, an experimental setup is developed using a single-phase and three-phase compatible PWM converter along with a human body impedance model, as illustrated in Fig. 17. The power converter operates at a switching frequency of 20 kHz, which significantly exceeds the grid frequency of 60 Hz. The EMI filter is configured as a third-order CM and DM filter with a 500-nF Y-capacitor. The PE wire is connected to the Y-capacitor, and the HBM hardware is set to simulate the touching conditions. Fig. 18 presents the overall system diagram for the proposed control and modulation methods. The PE current is measured using a hall-type leakage current sensor and is converted by the analog-to-digital converter (ADC) module within a digital signal processor (DSP). Employing the PE current as feedback, the proposed CMV controller is implemented within the DSP. In addition, a DM current controller is simultaneously operated to adjust the dc-link voltage and output power [44]. To estimate the phase angle, a second-order generalized integrator quadrature signal generator based phase-locked loop is employed. A synchronous reference frame current controller is utilized for both single-phase and three-phase PWM converters. Moreover, the resonant current controller is integrated to ensure constant power transfer at grid voltage fluctuation, such as voltage sag and harmonics. The output of the CM and DM current controller is applied as the CMV and DMV reference for the PWM converter. At last, the CMV and DMV references are synthesized by the proposed HDSVPWM. For the single-phase topology, the c phase is neglected. In addition, the TC i_{tc} is measured using the HBM hardware and compared

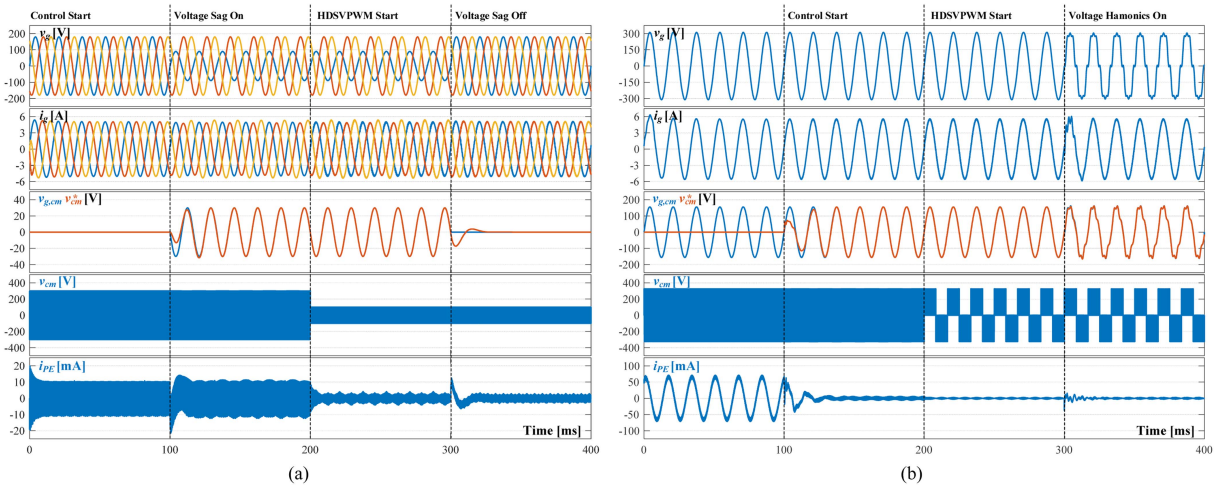

Fig. 19. Simulated waveform of transformerless AC–DC converter operating at grid voltage variation. (a) CMV control and HDSVPWM for three-phase PWM converter with grid voltage sag. (b) CMV control and HDSVPWM for single-phase PWM converter with grid voltage harmonics.

against the TC regulation defined by the IEC 61851-1 standard, which is relevant for the EV charging applications [45].

A. Simulation Results

The proposed CMV controller and HDSVPWM are verified by the three-phase and single-phase transformerless ac–dc power conversion systems. Fig. 19(a) illustrates the simulated waveform of the three-phase PWM converter operating under the three-phase wye grid with TT neutral grounding system, where the ground impedance is high. Under the normal operating conditions, the grid frequency CMV is nearly zero, leaving only HF leakage currents. In contrast, when a 50% grid voltage sag is presented at one phase, the grid frequency CMV of (1) is produced. This generates the LF leakage currents, which flow into the PE wire. However, with the application of the proposed CMV controller, the PE current is directly measured, and the LF CMV is injected by the PWM converter. The CMV reference closely resembles the grid voltage, resulting in a rapid reduction of the LF leakage currents. Subsequently, the proposed three-phase HDSVPWM is applied, utilizing the voltage vectors with only two levels of the instantaneous CMV. As a result, both low- and HF leakage currents are suppressed at the same time. When the grid voltage sag ends and the normal operation resumes, the CMV reference rapidly decreases to zero.

In Fig. 19(b), the single-phase PWM converter is operated under the single-phase grid with TT end-of-phase grounding system, where the ground impedance is high. Unlike in the three-phase system, a significant grid frequency CMV, as derived by (1), is always present during normal operations. The magnitude of the CMV is approximately a half of the grid voltage, resulting in much higher leakage currents compared to the three-phase case. However, upon applying the proposed CMV control, the LF leakage currents are rapidly reduced within one cycle. Furthermore, the HF leakage currents are suppressed immediately upon activation of the proposed single-phase HDSVPWM. The 3rd, 5th, and 7th grid voltage harmonics, each with a magnitude

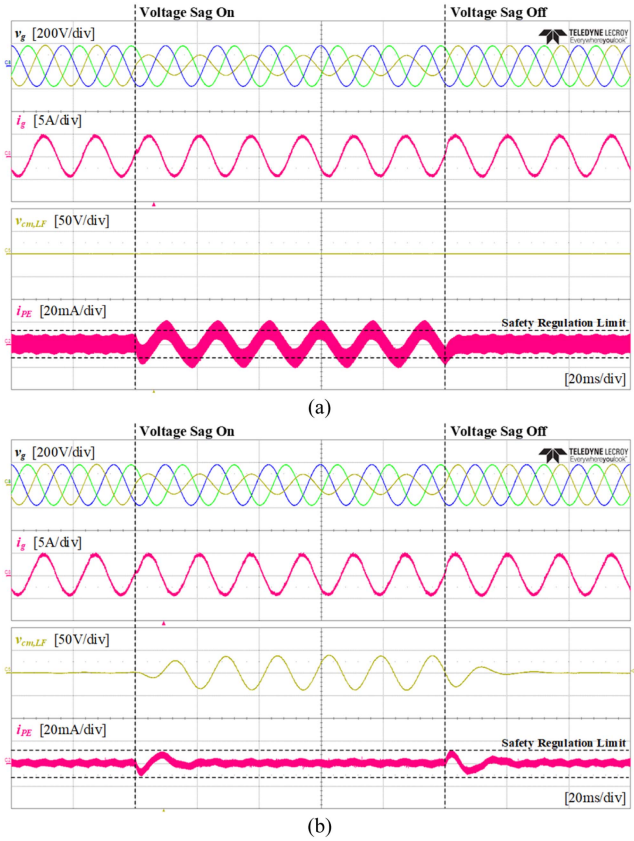

Fig. 20. Experimental waveform of three-phase PWM converter with grid voltage sag condition. (a) Without CMV control. (b) With proposed CMV control and HDSVPWM.

of 10% of the fundamental, are applied using the grid simulator. When grid voltage harmonics are present, CMV at the corresponding harmonic frequencies is generated. Nevertheless, the LF CMV reference is rapidly adjusted, and the leakage currents are effectively attenuated, as the proposed CMV control method is specifically designed to target the grid fundamental and harmonic frequencies. As a result, both LF and HF leakage

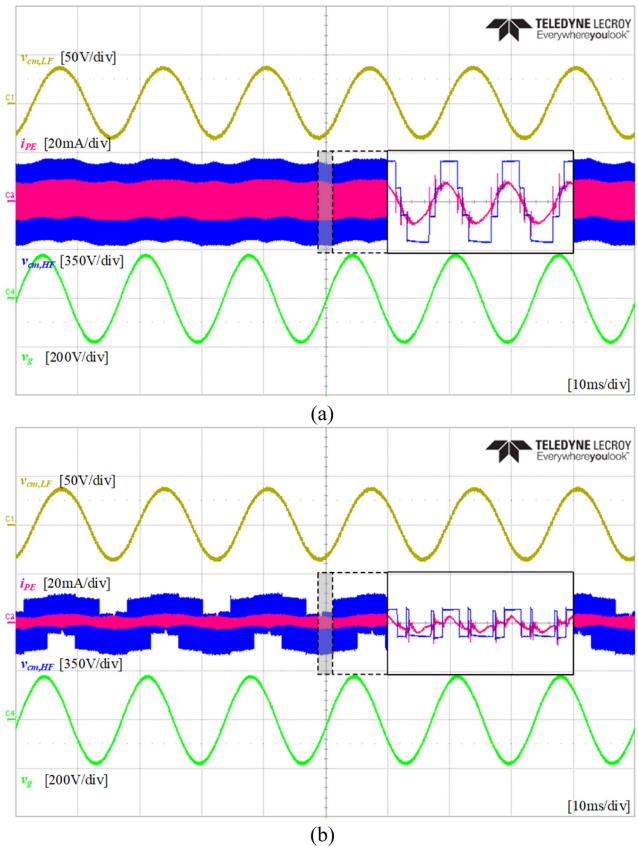

Fig. 21. Experimental waveform of LF CMV injection in three-phase PWM converter. (a) Conventional PWM. (b) Proposed HDSVPWM.

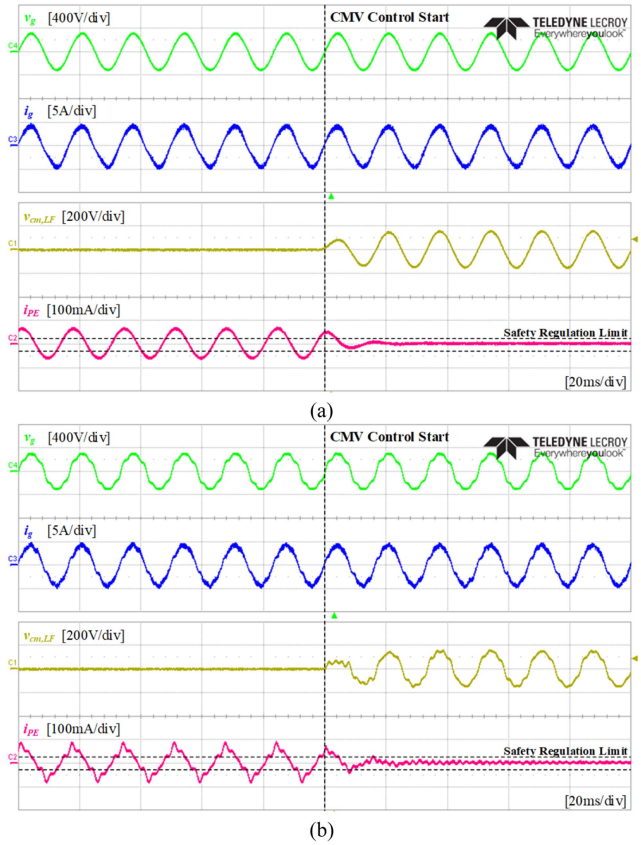

Fig. 22. Experimental waveform of CMV control method for single-phase PWM converter. (a) Normal operation. (b) Grid harmonics operation.

currents are mitigated at the single/three-phase PWM converters by utilizing the proposed CMV control method and HDSVPWM simultaneously.

B. Experimental Results

The proposed control and modulation methods are verified by the experimental setup for the three-phase and single-phase PWM converters. For the three-phase experiments, a three-phase grid simulator is utilized to implement 220 VAC three-phase grid. The PE wire is connected to the utility ground with the ground impedance determined according to the specific grounding method. The leakage current sensor is placed at the PE wire to directly measure the leakage current. Fig. 20 shows the experimental waveform of the three-phase PWM converter under a 50% grid voltage sag condition. The grid voltage sag generated a grid frequency CMV similar to the waveform described in Fig. 19(a). Without the CMV control, the LF leakage currents, proportional to the grid voltage variation, are generated with a peak of 20 mA, as shown in Fig. 20(a). Therefore, the human safety issue occurs, exceeding the regulation limit, which is derived from a TC limit in the IEC 61851-1 standard. However, after applying the proposed CMV controller, the LF leakage currents are measured by the leakage current sensor and employed as feedback. Then, the LF CMV is injected through the PWM converter, mitigating the LF leakage currents within one cycle, as depicted in Fig. 20(b). The waveform of the phase current remains constant with the CMV control, indicating that the CMV injection does not interfere with the ac–dc power conversion. In Fig. 21, the conventional PWM and the proposed three-phase HDSVPWM are compared during the LF injection. While the amount of the LF CMV is identical, the proposed HDSVPWM exhibits a lower CMV ripple with only two levels of the HF CMV. Notably, even with the application of dead-time in the actual PWM converter, no CMV spike occurs, and the instantaneous CMV is generated as desribed in Fig. 14. Accordingly, the leakage currents are reduced with a peak of 4 mA when the HDSVPWM is applied. As a result, both LF and HF leakage currents are attenuated by the proposed CMV controller and HDSVPWM for the three-phase PWM converter.

In Fig. 22, the proposed control and modulation methods are implemented in the single-phase ac–dc power conversion system with a 220-VAC single-phase grid simulator. The magnitude of grid frequency CMV is higher than the three-phase topology, resulting in substantial leakage currents with a peak of 70 mA, as illustrated in Fig. 22(a). However, when the proposed CMV control method is applied to the single-phase PWM converter, the injection of the LF CMV leads to a rapid attenuation of the leakage currents to meet the regulation within one cycle. Similar to the case of the three-phase application, the CMV control is conducted independent of the ac–dc power conversion, maintaining a uniform waveform of the phase current. The 3rd,

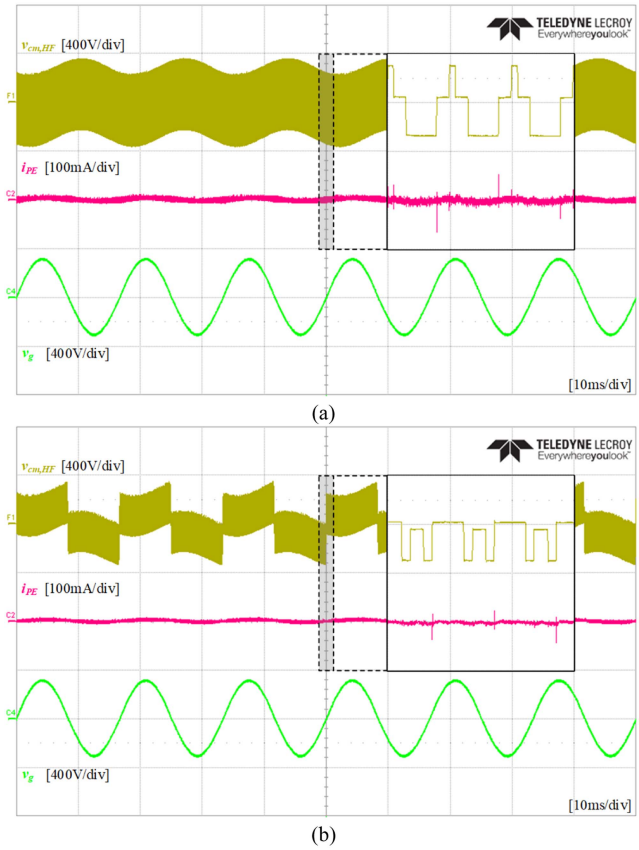

Fig. 23. Experimental waveform of LF CMV injection in single-phase PWM converter. (a) Conventional PWM. (b) Proposed HDSVPWM.

5th, and 7th grid voltage harmonics, each with a magnitude of 10% of the fundamental, are applied using the grid simulator, as described in Fig. 22(b). As shown in Fig. 7, the impact of the LF CMV increases exponentially with rising frequency, leading to a substantial magnitude of the leakage currents. Furthermore, unlike in the three-phase system, each grid harmonic voltage generates significant LF CMV without any harmonic cancellation. Nevertheless, the CMV reference is generated with the grid harmonic frequency, which is closely similar to the grid frequency CMV. Therefore, the LF leakage currents are mitigated under the CMV control, satisfying the safety regulation limit. Fig. 23 illustrates the waveform of the conventional PWM method and the proposed single-phase HDSVPWM during a LF CMV injection. While the amount of LF CMV is identical, the proposed HDSVPWM displays a lower CMV ripple. The expanded waveform shows an injection of the negative CMV using only two levels of instantaneous CMV with a voltage ripple of $0.5v_{dc}$ in the HDSVPWM. Notably, even with the application of dead-time in the actual PWM converter, no CMV spike occurs, and the instantaneous CMV is generated as described in Fig. 16. The peak of the leakage currents is attenuated to 3 mA when the HDSVPWM is conducted. Consequently, both LF and HF leakage currents are effectively suppressed by the proposed CMV control and HDSVPWM for the single-phase PWM converter.

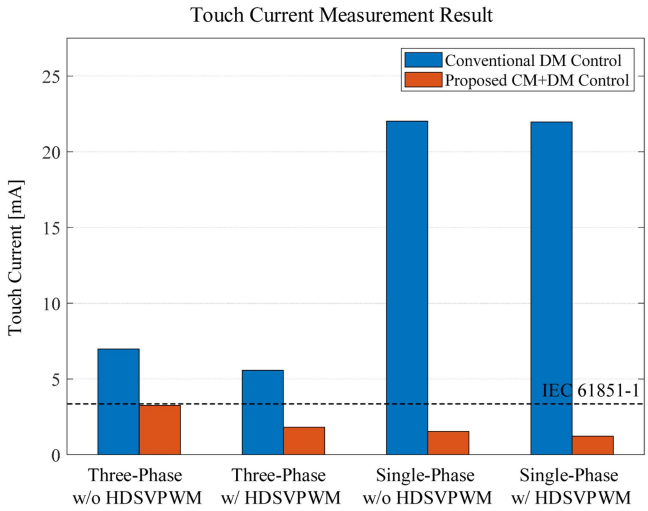

Fig. 24. Experiment results of TC measurement at three-phase and single-phase topology with proposed HDSVPWM.

The TC is measured using the HBM hardware under various operating conditions, as depicted in Fig. 24. According to the IEC 61851-1 standard, the TC is required to be attenuated below 5 mA. With the conventional DM control for the PWM converter, the TC exceeds the limit at both three-phase and single-phase applications. However, when the proposed CMV controller is conducted, the TC is effectively suppressed below the regulatory threshold. In addition, the TC is further reduced when the proposed HDSVPWM is applied. Since the HBM inherently functions as a low-pass filter, the effect of the leakage current suppression at the LF is greater. Consequently, the proposed CMV control method and HDSVPWM effectively enhance the human safety of the transformerless ac–dc power conversion system.

VI. Conclusion

The removal of isolation barrier in the transformerless system presents a significant challenge regarding the leakage currents. This article proposes the control and modulation methods of the single-/three-phase PWM converter to suppress both LF and HF leakage currents. The contributions are as follows.

1) The effect of the CMV sources on the leakage currents is analyzed through the CM equivalent circuit, considering the practical EMI filter and grounding system.
2) Based on the plant model, the CMV control method is introduced to attenuate the LF leakage currents. Utilizing the leakage current as feedback, the controller is designed to generate a CMV reference. The performance and stability of the controller are verified analytically.
3) The HDSVPWM is proposed to synthesize both CMV and DMV references while minimizing HF CMV ripple. The HF CMV generated by the voltage vector is analyzed in the single-/three-phase PWM converter, mitigating the HF leakage currents.

The effectiveness of the proposed methods is demonstrated by the experimental results, using the ac grid simulator and the single-/three-phase PWM converter. Furthermore, the TC is

evaluated by the HBM hardware, ensuring a compliance with the safety regulation. Consequently, the proposed CMV controller and HDSVPWM provide a practical solution for transformerless ac–dc power conversion systems, offering a reliable approach for the industrial applications such as EV chargers, microgrids, and renewable energy systems.

APPENDIX

In the proposed single-phase HDSVPWM, the CMV and DMV references are expressed as a single vector in (19). It is important to note that the CMV and DMV references are orthogonal in the space vector plane, as these voltages are independent of each other. The DMV and CMV components of each voltage vector are given by

$$\begin{aligned} S_{Vk} &\equiv (x,y)\ k = 1,\ 2,\ 3,\ 4, \\ v_{dm} &= \frac{x-y}{4}\, v_{\rm dc}, \\ v_{cm} &= \frac{x+y}{4}\, v_{\rm dc} \end{aligned} \tag{A1}$$

and the corresponding switching states of each voltage vector S_{Vk} are listed in Table III. During one switching period, multiple voltage vectors are utilized to synthesize the reference voltage. Specifically, the duration of each voltage vector t_{Vk} is determined and the sum of the durations equals the switching period $t_{\rm sw}$. Therefore, the relationship between the voltage reference and the duration of each voltage vector is derived as

$$\frac{t_{\rm sw}}{v_{\rm dc}} \begin{pmatrix} v_{\rm dm} \\ v_{\rm cm} \\ v_{\rm dc} \end{pmatrix} = \begin{pmatrix} 0.5 & 0 & -0.5 & 0 \\ 0 & 0.5 & 0 & -0.5 \\ 1 & 1 & 1 & 1 \end{pmatrix} \begin{pmatrix} t_{V1} \\ t_{V2} \\ t_{V3} \\ t_{V4} \end{pmatrix}. \tag{A2}$$

The rank of the transfer matrix $\mathbf{T_{3\times 4}}$ is three, indicating that its column space is not a full rank. In other words, only three voltage vectors are required to synthesize the reference voltage. As utilizing fewer voltage vectors reduces the number of switching, the proposed single-phase HDSVPWM utilizes only three out of four vectors. For instance, if the voltage vector V_4 is excluded, (A2) is modified as follows:

$$\frac{t_{\rm sw}}{v_{\rm dc}} \begin{pmatrix} v_{\rm dm} \\ v_{\rm cm} \\ v_{\rm dc} \end{pmatrix} = \begin{pmatrix} 0.5 & 0 & -0.5 \\ 0 & 0.5 & 0 \\ 1 & 1 & 1 \end{pmatrix} \begin{pmatrix} t_{V1} \\ t_{V2} \\ t_{V3} \end{pmatrix} \tag{A3}$$

resulting in a square transfer matrix $\mathbf{T_{3\times 3}}$ with full rank. Since the transfer matrix is nonsingular, the duration of the voltage vector is directly calculated using the inverse matrix of $\mathbf{T_{3\times 3}}$. Therefore, the reference vector is synthesized using three voltage vectors, forming a triangular space vector region. The method for selecting the appropriate triangular region is detailed in the main text. Once the space vector region is determined, the durations of the selected voltage vectors are calculated. For instance, the durations of the voltage vectors in the upper triangular region are derived by (A3), which results in (20).

In the proposed three-phase HDSVPWM, the CMV and DMV references are expressed as a single vector in (16). Similar to the case of the single-phase PWM, the CMV and DMV references are orthogonal in the space vector plane. The voltage vector listed in Table II has a corresponding value of *dq* DMV and CMV. In addition, the duration of each voltage vector t_{Vk} is determined and the sum of the durations equals the switching period $t_{\rm sw}$. Therefore, the relationship between the voltage reference and the duration of each voltage vector is derived as

$$\frac{t_{\rm sw}}{v_{\rm dc}} \begin{pmatrix} v_{{\rm dm},d} \\ v_{{\rm dm},q} \\ v_{\rm cm} \\ v_{\rm dc} \end{pmatrix} = \mathbf{T_{4\times 8}} \begin{pmatrix} t_{V0} \\ t_{V1} \\ t_{V2} \\ t_{V3} \\ t_{V4} \\ t_{V5} \\ t_{V6} \\ t_{V7} \end{pmatrix} = \mathbf{T_{4\times 8}}\ \mathbf{V}_{8\times 1} \tag{A4}$$

where $\mathbf{V_{8\times 1}}$ represents the matrix of voltage vector durations. Following the same approach as the single-phase HDSVPWM, four voltage vectors are utilized for the voltage synthesis, which represents the minimum required number. Therefore, (A4) is modified into

$$\frac{t_{\rm sw}}{v_{\rm dc}} \begin{pmatrix} v_{{\rm dm},d} \\ v_{{\rm dm},q} \\ v_{\rm cm} \\ v_{\rm dc} \end{pmatrix} = \mathbf{T_{4\times 4}}\ \mathbf{V_{4\times 1}} \tag{A5}$$

where the transfer matrix $\mathbf{T_{4\times 4}}$ has full rank and is nonsingular. Therefore, the duration of the voltage vector is directly calculated using the inverse matrix of $\mathbf{T_{4\times 4}}$. Therefore, the reference vector is synthesized using four voltage vectors, forming a tetrahedron space vector region. The method for selecting the appropriate tetrahedron region is detailed in the main text. Once the space vector region is determined, the durations of the selected voltage vectors are derived by (A5).

REFERENCES

[1] S. Rivera et al., "Charging infrastructure and grid integration for electromobility," *Proc. IEEE*, vol. 111, no. 4, pp. 371–396, Apr. 2023.

[2] Q. Liu, T. Caldognetto, and S. Buso, "Review and comparison of grid-tied inverter controllers in microgrids," *IEEE Trans. Power Electron.*, vol. 35, no. 7, pp. 7624–7639, Jul. 2020.

[3] M. N. H. Khan, M. Forouzesh, Y. P. Siwakoti, L. Li, T. Kerekes, and F. Blaabjerg, "Transformerless inverter topologies for single-phase photovoltaic systems: A comparative review," *IEEE J. Emerg. Sel. Topics Power Electron.*, vol. 8, no. 1, pp. 805–835, Mar. 2020.

[4] J. Wang et al., "Nonisolated electric vehicle chargers: Their current status and future challenges," *IEEE Electrific. Mag.*, vol. 9, no. 2, pp. 23–33, Jun. 2021.

[5] D. Dong, I. Cvetkovic, D. Boroyevich, W. Zhang, R. Wang, and P. Mattavelli, "Grid-interface bidirectional converter for residential DC distribution systems—Part one: High-density two-stage topology," *I IEEE Trans. Power Electron.*, vol. 28, no. 4, pp. 1655–1666, Apr. 2013.

[6] G.-H. Min, H. Kwon, J. Lee, and J.-I. Ha, "Virtually isolated class E converter with coupled capacitors," in *Proc. IEEE Appl. Power Electron. Conf. Expo.*, 2023, pp. 2124–2128.

[7] C. Stutz, S. Nielebock, and M. März, "Applying a fast analytic calculation method in CM domain for touch currents to a two-stage charging infrastructure," in *Proc. 25th Eur. Conf. Power Electron. Appl.*, 2023, pp. 1–10.

[8] C. Yao, X. Zhang, Y. Zhang, P. Yang, H. Li, and J. Wang, "Semiconductor-based galvanic isolation: Touch current suppression," *IEEE Trans. Power Electron.*, vol. 35, no. 1, pp. 48–58, Jan. 2020.

[9] S. Dey, A. Mallik, and S. Mishra, "A mathematical design approach to volumetric optimization of EMI filter and modeling of CM noise sources in a three-phase PFC," *IEEE Trans. Power Electron.*, vol. 37, no. 1, pp. 462–472, Jan. 2022.
[10] D. Zhang, M. Leibl, J. Mühlethaler, J. Huber, and J. W. Kolar, "Analytical modeling and comparison of EMI pre-filter noise emissions of three-phase voltage and current DC-link converters," *IEEE Trans. Power Electron.*, vol. 39, no. 11, pp. 14691–14707, Nov. 2024.
[11] D. Dong, F. Luo, X. Zhang, D. Boroyevich, and P. Mattavelli, "Grid-interface bidirectional converter for residential DC distribution systems—Part 2: AC and DC interface design with passive components minimization," *IEEE Trans. Power Electron.*, vol. 28, no. 4, pp. 1667–1679, Apr. 2013.
[12] L. Zhou, M. Jahnes, M. Eull, W. Wang, and M. Preindl, "Control design of a 99% efficiency transformerless EV charger providing standardized grid services," *IEEE Trans. Power Electron.*, vol. 37, no. 4, pp. 4022–4038, Apr. 2022.
[13] F. Chen, R. Burgos, and D. Boroyevich, "A bidirectional high-efficiency transformerless converter with common-mode decoupling for the interconnection of AC and DC grids," *IEEE Trans. Power Electron.*, vol. 34, no. 2, pp. 1317–1333, Feb. 2019.
[14] L. Wang, X. Zhang, X. Han, Y. Ren, B. Zhang, and P. Wang, "A transformerless converter with common-mode decoupling in low-voltage hybrid grids," *Processes*, vol. 12, no. 3, 2024, Art. no. 507.
[15] D.-I. Lee, S.-M. Hong, J.-B. Lee, H.-S. Youn, D.-W. Lee, and Y.-S. Lee, "Non-isolated on-board charger capable of reducing common mode leakage current and balancing voltage of Y-capacitor on high voltage battery," *IEEE Trans. Transport. Electrific.*, to be published, doi: 10.1109/TTE.2024.3512578.
[16] T. R. Oliveira, W. W. A. G. Silva, S. I. Seleme, and P. F. Donoso-Garcia, "PLL-based feed-forward control to attenuate low-frequency common-mode voltages in transformerless LVDC systems," *IEEE Trans. Ind. Appl.*, vol. 55, no. 3, pp. 3151–3159, May/Jun. 2019.
[17] R. Zhu, G. Buticchi, and M. Liserre, "Investigation on common-mode voltage suppression in smart transformer-Fed distributed hybrid grids," *IEEE Trans. Power Electron.*, vol. 33, no. 10, pp. 8438–8448, Oct. 2018.
[18] J. Huang and H. Shi, "Suppressing low-frequency components of common-mode voltage through reverse injection in three-phase inverter," *IET Power Electron.*, vol. 7, no. 6, pp. 1644–1653, 2014.
[19] D. O. Boillat, F. Krismer, and J. W. Kolar, "Ground current control scheme for back-to-back three-phase T-type rectifier and inverter systems," *IEEJ Trans. Electr. Electron. Eng.*, vol. 13, no. 11, pp. 1649–1653, 2018.
[20] X. Li, X. Xing, C. Zhang, A. Chen, C. Qin, and G. Zhang, "Simultaneous common-mode resonance circulating current and leakage current suppression for transformerless three-level T-type PV inverter system," *IEEE Trans. Ind. Electron.*, vol. 66, no. 6, pp. 4457–4467, Jun. 2019.
[21] D. Zhang, D. Cao, J. Huber, J. Everts, and J. W. Kolar, "Nonisolated three-phase current DC-link buck–Boost EV charger with virtual output midpoint grounding and ground current control," *IEEE Trans. Transport. Electrific.*, vol. 10, no. 1, pp. 1398–1413, Mar. 2024.
[22] L. Xie and X. Yuan, "Common-mode current reduction at DC and AC sides in inverter systems by passive cancellation," *IEEE Trans. Power Electron.*, vol. 36, no. 8, pp. 9069–9079, Aug. 2021.
[23] R. T. H. Li, C. N. M. Ho, and E.-X. Chen, "Active virtual ground—Single-phase transformerless grid-connected voltage source inverter topology," *IEEE Trans. Power Electron.*, vol. 33, no. 2, pp. 1335–1346, Feb. 2018.
[24] J. Dadkhah, C. N. M. Ho, and K. K.-M. Siu, "Three-phase transformerless PV inverter with reconfigurable LCL filter and reactive power capability," *IEEE Trans. Power Electron.*, vol. 39, no. 7, pp. 8229–8241, Jul. 2024.
[25] F. Akbar, A. Elkhateb, H. F. Ahmed, A. A. Khan, H. Cha, and J.-W. Park, "Single-phase virtual-ground transformerless buck–Boost inverters," *IEEE Trans. Power Electron.*, vol. 38, no. 9, pp. 11585–11600, Sep. 2023.
[26] J.-H. Jung, S.-I. Hwang, and J.-M. Kim, "A common-mode voltage reduction method using an active power filter for a three-phase three-level NPC PWM converter," *IEEE Trans. Ind. Appl.*, vol. 57, no. 4, pp. 3787–3800, Jul./Aug. 2021.
[27] M. H. Hedayati and V. John, "Filter configuration and PWM method for single-phase inverters with reduced conducted EMI noise," *IEEE Trans. Ind. Appl.*, vol. 51, no. 4, pp. 3236–3243, Jul./Aug. 2015.
[28] R. Shen and H. S.-H. Chung, "Mitigation of ground leakage current of single-phase PV inverter using hybrid PWM with soft voltage transition and nonlinear output inductor," *IEEE Trans. Power Electron.*, vol. 36, no. 3, pp. 2932–2946, Mar. 2021.
[29] S. J. Lee, J. Choi, G. C. Lim, S. M. Kim, E.-K. Kim, and J.-I. Ha, "Analysis and mitigation of bearing current in inverter-fed IPMSMs drive system," *IEEE Trans. Ind. Electron.*, to be published, doi: 10.1109/tie.2024.3456435.
[30] A. M. Hava and E. Un, "Performance analysis of reduced common-mode voltage PWM methods and comparison with standard PWM methods for three-phase voltage-source inverters," *IEEE Trans. Power Electron.*, vol. 24, no. 1, pp. 241–252, Jan. 2009.
[31] J. Xu, J. Han, Y. Wang, S. Habib, and H. Tang, "A novel scalar PWM method to reduce leakage current in three-phase two-level transformerless grid-connected VSIs," *IEEE Trans. Ind. Electron.*, vol. 67, no. 5, pp. 3788–3797, May 2020.
[32] J. Lee and J.-W. Park, "Selection of PWM methods for common-mode voltage and DC-link capacitor current reduction of three-phase VSI," *IEEE Trans. Ind. Appl.*, vol. 59, no. 1, pp. 1064–1076, Jan./Feb. 2023.
[33] K. Nanshikar and S. Das, "Optimal space vector-based hybrid PWM scheme in terms of common-mode voltage and line current ripple," *IEEE Trans. Power Electron.*, vol. 39, no. 11, pp. 14478–14492, Nov. 2024.
[34] M. Lak, B.-R. Chuang, and T.-L. Lee, "A common-mode voltage elimination method with active neutral point voltage balancing control for three-level T-type inverter," *IEEE Trans. Ind. Appl.*, vol. 58, no. 6, pp. 7499–7514, Nov./Dec. 2022.
[35] *Low-voltage Electrical Installations - Part 1: Fundamental principles, Assessment of General Characteristics, Definitions*, IEC Standard 60364-1, 2005.
[36] *Methods of Measurement of Touch Current and Protective Conductor Current*, IEC Standard 60990, 2016.
[37] J. Lee, D. Lee, S. Lee, and J.-I. Ha, "Direct leakage current control method of single-phase non-isolated EV charger," in *Proc. IEEE 10th Int. Power Electron. Motion Control Conf.*, 2024, pp. 5053–5058, doi: 10.1109/ipemc-ecceasia60879.2024.10567233.
[38] M. S. Elkayam and A. Kuperman, "Guidelines for single-parameter multiresonant current controllers design allowing prescribed magnitude tracking of periodic references," *IEEE Trans. Power Electron.*, vol. 36, no. 8, pp. 9536–9546, Aug. 2021.
[39] A. G. Yepes, F. D. Freijedo, O. Lopez, and J. Doval-Gandoy, "Analysis and design of resonant current controllers for voltage-source converters by means of Nyquist diagrams and sensitivity function," *IEEE Trans. Ind. Electron.*, vol. 58, no. 11, pp. 5231–5250, Nov. 2011.
[40] N. El-Sherif, T. A. Domitrovich, and F. P. Reyes, "Ground-fault circuit interrupters: A standards perspective," *IEEE Ind. Appl. Mag.*, vol. 27, no. 1, pp. 55–68, Jan./Feb. 2021.
[41] Y. Wu, Z. Wei, Y. Yang, and P. Zhang, "Improved common-mode leakage current measurement method for insulation condition monitoring in distribution grids," *IEEE Trans. Ind. Electron.*, vol. 71, no. 5, pp. 5307–5317, May 2024.
[42] G. Tan, X. Wu, Z. Wang, and Z. Ye, "A generalized algorithm to eliminate spikes of common-mode voltages for CMVRPWM," *IEEE Trans. Power Electron.*, vol. 31, no. 9, pp. 6698–6709, Sep. 2016.
[43] J. Huang and K. Li, "Eliminating common-mode voltage spikes caused by dead-time effect in three-phase inverters through symmetrical rotation reverse carriers," *IEEE Trans. Power Electron.*, vol. 36, no. 5, pp. 6056–6067, May 2021.
[44] J. Rocabert, A. Luna, F. Blaabjerg, and P. Rodríguez, "Control of power converters in AC microgrids," *IEEE Trans. Power Electron.*, vol. 27, no. 11, pp. 4734–4749, Nov. 2012.
[45] *Electric Vehicle Conductive Charging System—Part 1: General Requirements*, IEC Standard 61851-1, 2017.

Juwon Lee (Student Member, IEEE) was born in Seoul, South Korea, in 1997. He received the B.S. degree in electrical engineering in 2020 from Seoul National University, Seoul, South Korea, where he is currently working toward the Ph.D. degree in electrical engineering.

His current research interests include electric energy conversion, grid-connected converter, and design and control of transformerless ac–dc/dc–dc converter.

Dongsu Lee (Student Member, IEEE) was born in Seoul, South Korea, in 1996. He received the B.S. degree in automotive engineering in 2021 from Hanyang University, Seoul, South Korea, where he is currently working toward the Ph.D. degree in electrical engineering.

His research interests include nonisolated electric vehicle chargers, grid connected power-factor-correcting ac–dc converter, and motor drives.

Jung-Ik Ha (Fellow, IEEE) was born in South Korea, in 1971. He received the B.S., M.S., and Ph.D. degrees in electrical engineering from Seoul National University, Seoul, South Korea, in 1995, 1997, and 2001, respectively.

From 2001 to 2002, he was a Researcher with Yaskawa Electric Corporation, Kitakyushu, Japan. From 2003 to 2008, he worked as a Senior and Principal Engineer with Samsung Electronics Company, South Korea. From 2009 to 2010, he was the Chief Technology Officer with LS Mecapion Company, Daegu, South Korea. Since 2010, he has been with the Department of Electrical and Computer Engineering, Seoul National University, Seoul, South Korea, where he is currently a Professor. He is also with the Seoul National University Electric Power Institute. From 2016 to 2017, he was a Visiting Scholar with the Massachusetts Institute of Technology, Cambridge, MA, USA. He has authored more than 300 papers and patents published in power electronics and motor drives. His current research interests include circuits and control in high efficiency and integrated electric energy conversions for various industrial fields.